Supplemental Document

Biomedical Optics EXPRESS

Deep learning-based size prediction for optical trapped nanoparticles and extracellular vesicles from limited bandwidth camera detection: supplement

Derrick Boateng,[1] Kaiqin Chu,[2] Zachary J. Smith,[3,4] Jun Du,[1,6] and Yichuan Dai[4,5,7,]

[1]*National Engineering Research Center of Speech and Language Information Processing, Department of Electronic Engineering and Information Science, University of Science and Technology of China, China*
[2]*Suzhou Institute for Advanced Research, University of Science and Technology of China, China*
[3]*Key Laboratory of Precision Scientific Instrumentation of Anhui Higher Education Institutes, Department of Precision Machinery and Precision Instrumentation, University of Science and Technology of China, China*
[4]*Department of Precision Machinery and Precision Instrumentation, University of Science and Technology of China, China*
[5]*Department of Advanced Manufacturing, Nanchang University, China*
[6]*jundu@ustc.edu.cn*
[7]*daiyc@ustc.edu.cn*

Supplement DOI: https://doi.org/10.6084/m9.figshare.24542539

Parent Article DOI: https://doi.org/10.1364/BOE.501430

Deep Learning-Based Size Prediction for Optical Trapped Nanoparticles and Extracellular Vesicles from Limited Bandwidth Camera Detection

DERRICK BOATENG,[1] KAIQIN CHU,[2] ZACHARY J SMITH,[3,4] JUN DU*,[1] AND YICHUAN DAI*,[4,5]

[1]*National Engineering Research Center of Speech and Language Information Processing, Department of Electronic Engineering and Information Science, University of Science and Technology of China.*

[2]*Suzhou Institute for Advanced Research, University of Science and Technology of China.*

[3]*Key Laboratory of Precision Scientific Instrumentation of Anhui Higher Education Institutes, Department of Precision Machinery and Precision Instrumentation, University of Science and Technology of China.*

[4]*Department of Precision Machinery and Precision Instrumentation, University of Science and Technology of China.*

[5]*Department of Advanced Manufacturing, Nanchang University.*

* *jundu@ustc.edu.cn, daiyc@ustc.edu.cn.*

1. Configuration of Optical Tweezers System

A more detailed configuration of optical tweezer system is presented here. In the hardware section, elastically scattered light is collected by means of a 5% laser pickoff beamsplitter (BSF10-B, Thorlabs, New Jersey, USA) before the collection of sCMOS detector. An f = 500 mm lens (AC508-500-B-ML, Thorlabs, New Jersey, USA) is coupled with the camera. The images recorded by sCMOS are used to monitor the motion of trapped particles. Besides, considering the refractive index (RI) difference between samples, a neutral density filter was utilized in the high RI sample measurement to prevent pixel saturation. A bright-field CCD camera (DCU224M, Thorlabs, New Jersey, USA) allows visualization of the sample and assists optical trapping. In addition, a gradient neutral density filter（NDC-25C-4, Thorlabs）rotated by closed-loop step motor was applied for power reduction for strong and weak stiffness measurement. In the software section, devices including camera, shutter etc., are controlled via the program written by LabVIEW 2014 (National Instruments, Austin, USA). The user can define several parameters through the program interface, including the laser power, as well as frame rates and video length of optical tweezer camera.

2. Data Preprocessing of 1D position series extraction

The non-circular symmetric polarization of the laser makes the optical stiffness higher along the axis of stronger polarization. As a result, we can clearly see that the contour shape shown in Figure 1c in the main text is not circular but elliptical. We extracted the position distribution along two perpendicular directions, which was shown in Figure S1 a, and calculated the size along each direction based on Eq. (1) and (2), with their results as shown in Figure S1 b. It can be clearly seen that more accurate size is estimated from the "long axis" direction, for which the trapping stiffness is the lowest and nanoparticle motion most rigorously satisfies the diffusion approximation. Hence, the position series along long axis (blue line in Figure S1a) maintains the most accurate characteristics and were used as input of training network.

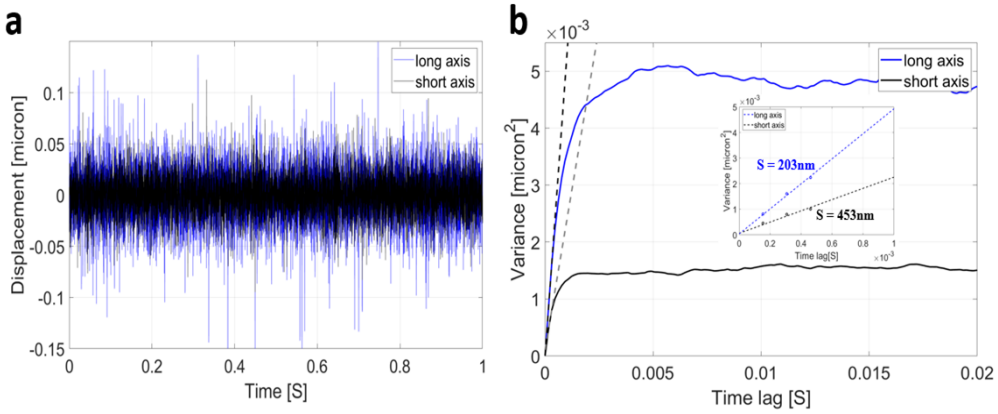

Figure S1 (a) Two position series extracted from perpendicular directions from 2D position series shown in Figure 1(c) in original text. (b) Variance of displacement versus time lag in each direction. Inset shows the linear fit through the first three points and corresponding size estimation results.

3. Sample Preparation and Nanoparticle Tracking Analysis (NTA)

For PS and Silica suspensions, original solutions were diluted > 10000 times and sonicated for 10 minutes to avoid aggregation. Finally, nanoparticle solutions were filtered using polycarbonate filters (Millipore) with 220 nm pore size. For the isolation of human platelet-free plasma (PFP) derived EVs, 100 µL of thawed PFP was diluted to 1 mL with PBS and transferred to a 3 mL ultracentrifuge tube of a Beckman Coulter Optima MAX-XP ultracentrifuge equipped with a TLA100.3 rotor. After the first ultracentrifugation step at 100 000g for 30 min at 4 °C, the pellet was washed with 1 mL of PBS for the second ultracentrifugation step at 100 000g for 17 min at 4 °C. Afterward, the PFP EVs were

resuspended in 50 μL of PBS for optical trapping.

NTA (NS300, Malvern, UK) was performed within the NTA chamber with approximately 1 mL solution. Before and after each measurement the sample chamber was rinsed with ultrapure water. Three consecutive 30-second videos were recorded for each sample. Shutter and gain settings were optimized for each sample. The number distributions were used to verify EVs size distributions in the main text section 3.3.

3. Optical Stiffness Determined by Thermal Motion Analysis

A trapped particle in the optical tweezers obey restricted Brownian motion near the center, with its position distribution probability density P(x) obeying Boltzmann's law and could be written as:

$$P(x) = \mathrm{c} * \exp\left(\frac{-\mathrm{E(x)}}{\mathrm{k}_B\mathrm{T}}\right) \tag{S1}$$

Where $\mathrm{E(x)}$ represents the potential of particle, c is a normalization constant. The potential near the center can be simplified as a simple harmonic potential, then P(x) could be further simplified as a Gaussian distribution representation：

$$P(x) = \mathrm{c} * \exp\left(\frac{-\mathrm{Kx}^2}{\mathrm{k}_B\mathrm{T}}\right) \tag{S2}$$

Here K represents trap stiffness. Hence, once a large number of the position is measured, stiffness K could be obtained by the position distribution probability fitting analysis. Figure S2 shows the thermal motion analysis of trapped individual PS200nm nanoparticle. To extract the actual potential E(x) from the histogram we calculate the logarithm of the frequency in Figure S2a and multiply it by k_BT (Figure S2b). This is fitted numerically by a harmonic potential with a stiffness constant K= 25 pN/μm.

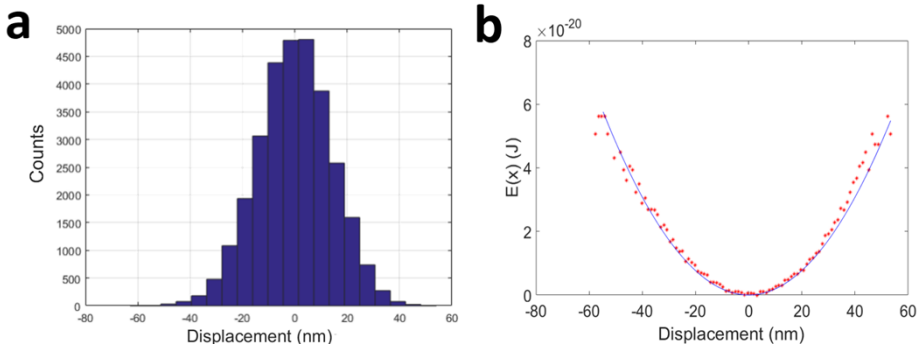

Figure S2 (a) Histogram of the PS200nm nanoparticle position fluctuation according to Figure 1a in the main text. (b) Energy profile for the trapped nanoparticle calculated from the histogram in (a) using Boltzmann statistic. The solid blue line shows a parabolic fit assuming a harmonically constrained Brownian particle.

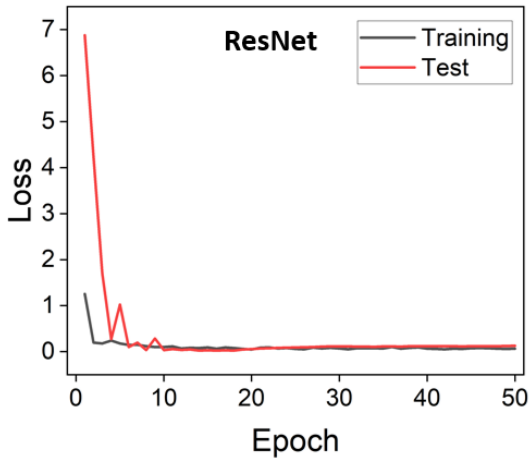

Figure S3 An example of the ResNet network training-testing loss curve.

4. Adjusted Lorentzian Fitting on Power Spectra Analysis

To acquire the size for a stable trapped nanoparticle, the adjusted Lorentzian model that accounts for motion blur, aliasing and potion detection error are applied for fitting to the power spectra acquired by camera-based position measurement, which could be written as[1]:

$$S_{ad}(f) = \sum_{n=-\infty}^{\infty} S\left(f + 2nf_{Nyq}\right) \times \left(\frac{\sin\left(W\pi\left(f + 2nf_{Nyq}\right)\right)}{W\pi\left(f + 2nf_{Nyq}\right)}\right)^2 + \varepsilon^2/2f_{Nyq} \quad \text{(S3)}$$

Where W, f_{Nyq} and ε^2 represent the acquisition time of camera, the Nyquist frequency (which equals to half of the sampling frequency) and position detection error of our optical tweezer system, S represents for typical power spectrum of the particle trapped in a harmonic potential well, which could be described by a Lorentzian model:

$$S(f) = \frac{k_b T}{2\pi^2\gamma(f^2 + f_c^2)} \quad \text{(S4)}$$

In which k_b and T are the Boltzmann constant and absolute temperature respectively, γ and f_c are the viscous drag coefficient and corner frequency, which could be written as a function of stiffness K and diameter d:

$$\gamma = 3\pi\eta d \quad \text{(S5)}$$

$$f_c = K/2\pi\gamma \quad \text{(S6)}$$

Prior knowledge is given based on the experimental acquisition settings and measurement. Specifically, we have W= 10μs, f_{Nyq}=3000Hz, ε^2=13.2nm^2, and K, d are the only parameters to be fitted. Adjusted Lorentzian fitting was performed in MATLAB using the 'lsqnonlin' function. Taking PS100nm nanoparticles as examples, the initial guess of the K, d is set as 10 pN/μm and 100nm respectively. The above parameters are set as the mean

based on priori experimental measurement for the highly heterogenous EVs, which is 30 pN/μm and 180nm, respectively. The summation is stopped at n= ± 3, sufficiently accounting for the blurring effect.

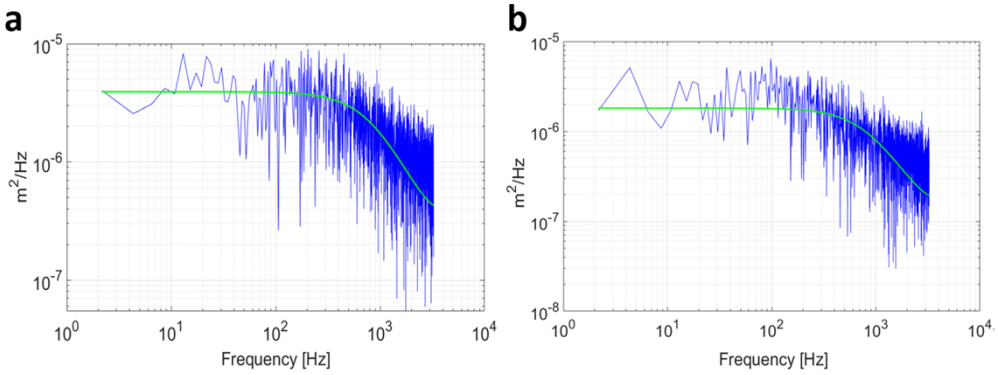

Figure S4 Measured power spectra (blue) with adjusted Lorentzian fits (green) for individual PS100nm (a) and EVs (b) respectively, the fit sizes are 113nm and 182nm respectively.

5. CNN-based Sizing Prediction Networks and its Performance

In the main text (Section 3.3), it was mentioned that we compare the performance of ResNet to different algorithms such as adjusted Lorentzian fitting or CNN-based sizing networks. Given that our datasets of constrained Brownian motion of trapped nanoparticles are one-dimensional, and the well-known ability of CNNs is to extract both global and local features, we adapted the 1D CNN-based regression model proposed in our previous work[2] for comparisons after slight modification to the output layer as shown schematically in Figure S4. Briefly, the network contains five convolutional layers in which filters are learned which extract the particle's dynamic features from the time series measurements of the particle position (input data). Each convolution layer learns a series of filters (8, 16, 32, 64, 64 filters in layers 1 through 5, respectively) with filter kernel sizes of 1×5. The convolutional layers are then followed by the batch normalization and rectified linear unit layers to enable better generalization and speed up the network training. The average pooling layer (Avg Pooling) with a pooling area of size 2 and stride of 2 is added after the first three convolution layers. At the end is the flatten layer, and finally a fully connected layer responsible for the regression.

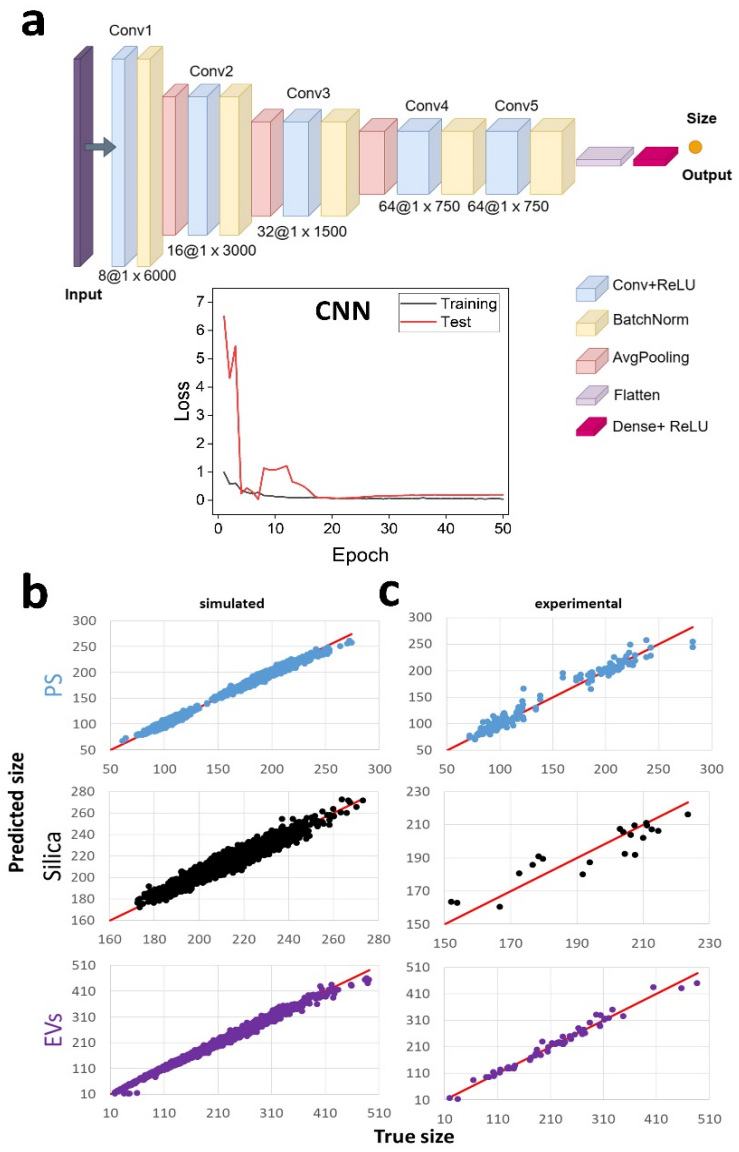

Figure S5 (a) CNN architecture for nanoparticles size prediction. Inset shows the network training-validation loss curve. CNN prediction performance using both simulated (b) and experimental (c) datasets of polystyrene (PS), silica nanospheres, and extracellular vesicles (EVs).

Table S1 RMSEP (nm) of the particle size predictions by CNN on the simulated and experimental datasets considering different time series lengths

	6000	3000	1000	6000	3000	1000

	Simulated	Simulated	Simulated	Experimental	Experimental	Experimental
PS100nm	2.94	4.28	6.45	7.61	9.20	12.95
PS200nm	5.91	7.60	14.02	11.47	12.52	18.10
Silica	4.34	5.92	9.19	8.42	10.01	12.29
EVs	13.19	14.49	16.92	20.19	29.86	34.79

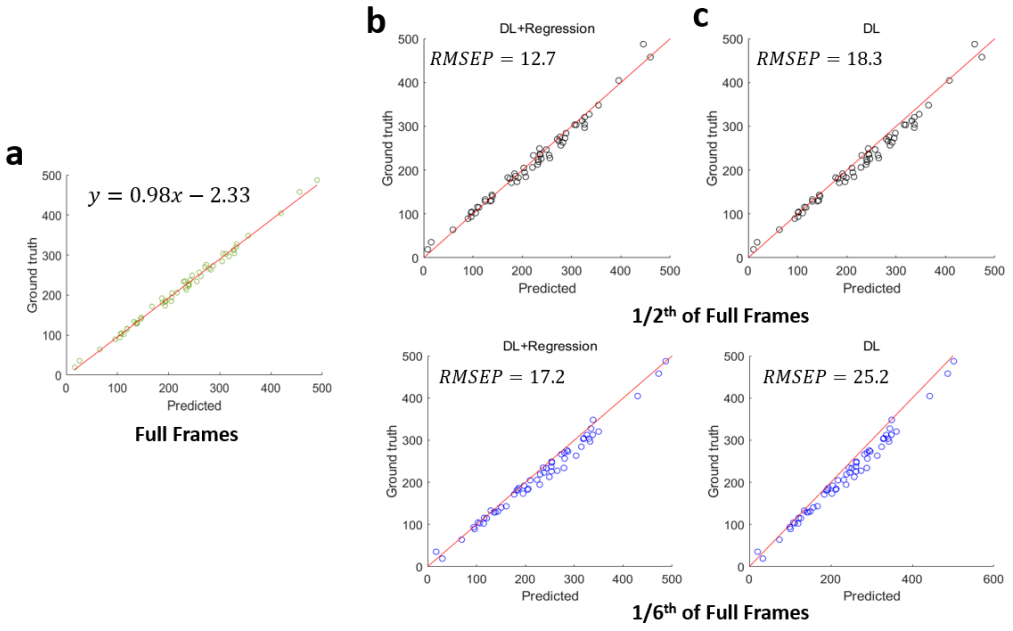

Figure S6 (a) Establishment of a linear regression model to restore the sizing performance of experimental EVs data. (b-c) Based on the model determined by (a), the restored sizing performance of experimental EVs data when using 1/2 or 1/6th of the full frames. Red lines represent lines of perfect agreement.

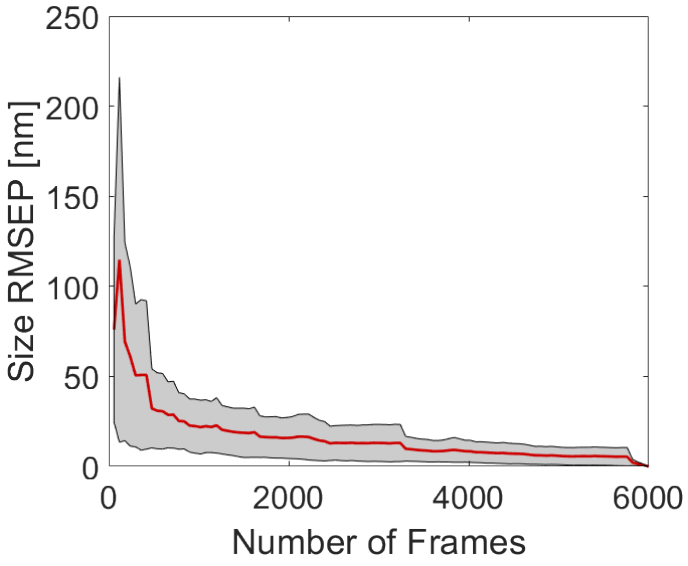

Figure S7 The relationship between sizing RMSEP and number of frames used for EVs calculation under weak-stiffness trapping condition (red line), the shaded regions indicate the standard deviation for the whole datasets.

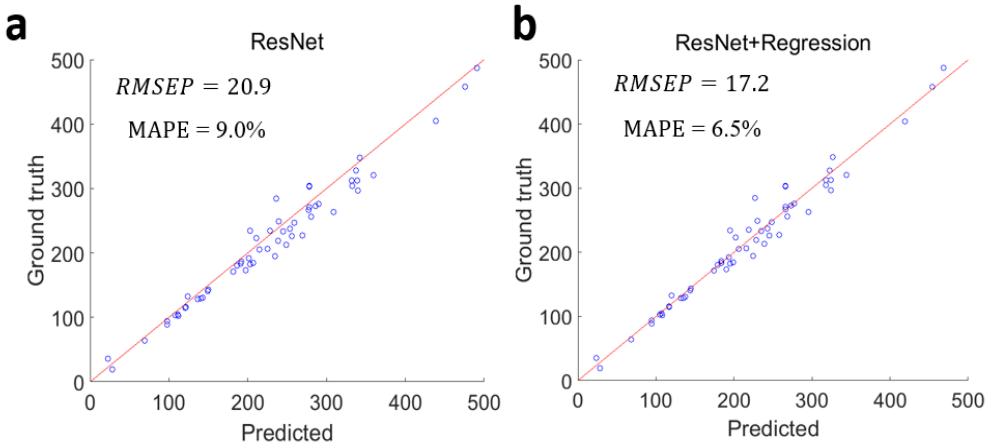

Figure S8 (a) Experimental Sizing performance of re-trained ResNet network by using the 120000 1000-frames simulated EVs. (b) Additional linear regression was used to restore the sizing performance. The regression model used here is identical to the previous model shown in Figure S6 (a). Red lines represent lines of perfect agreement.

6. EVs Refractive Index Analysis based on Mie Theory

Since the difference in scattering intensities for the particle size and focal volumes are negligible in our optical tweezer system, standard Mie theory instead of Generalized

Lorenz-Mie Theory[3] (GLMT) was employed for refractive index quantitative analysis. The backward scattering intensity collected by sCMOS camera could be written as:

$$I_{BS} = \frac{2\pi\alpha_{BS}}{k^2}\int_{\theta_{min}}^{\pi}\frac{1}{2}(|S_1|^2 + |S_2|^2)\sin\theta d\theta$$

Where parameters S_1 and S_2 are the scattering matrix elements and calculated using the MATLAB routines of Mätzler[4], k and θ represent wave number and polar angle, respectively, and θ is limited by numerical aperture (NA=$n_m sin\alpha$) of the objective. where n_m is the refractive index of the medium and α is the maximum propagation angle, $\theta_{min} = \pi - \sin^{-1}\alpha$. And the scalar α_{BS} is introduced in order to take the power of the laser beam and the camera setting into account in the numerical computations. Practically, the calibration of this factor is done by matching theoretical Mie scattering intensities with experimental measurements on NIST standard nanoparticles, as shown in Figure S7 a. Backward scattering intensity of trapped nanoparticles could be quantified by using the 16-bit images collected by sCMOS camera, while it is fluctuated due to axial constrained Brownian motion. To reduce the Poisson noise, we delete intensity outliers during time (I> Mean ± 3STD) and regard that nanoparticle is at focus when the maximum scattering intensity is detected. To avoid pixel saturation, a neutral density filter is employed when measuring PS200nm nanoparticles.

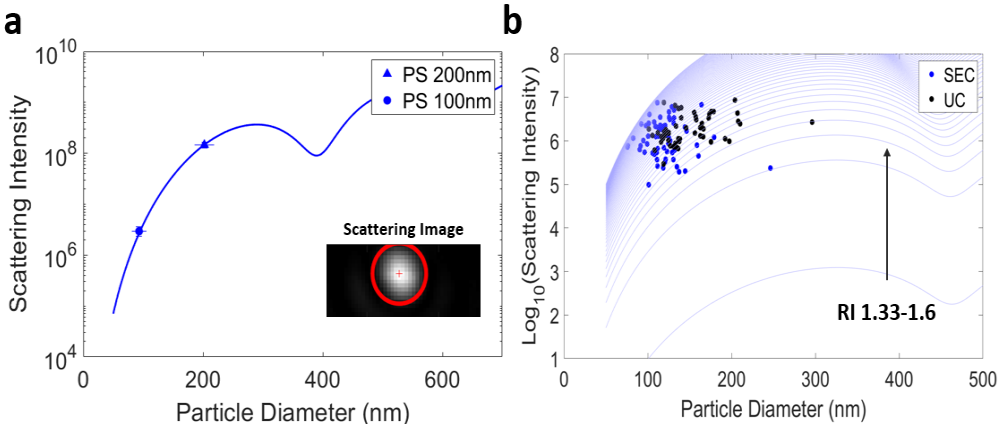

Figure S9 (a) Fitting between Scattering intensity of polystyrene beads to Mie theory curves, inset shows accumulation region based on centroid of particle image. Error bars indicate one standard deviation of the mean. (b) RI of plasma-derived EVs separated by UC and SEC along with gradient Mie theory curves, using the scalar fitting coefficient determined in (a).

Table S2 The average Size and Refractive index (RI) of PFP-derived vesicles predicted by ResNet

	SEC	UC
Size(nm)	120±25	155±36
RI	1.42±0.06	1.40±0.04

References

1. A. van der Horst and N. R. Forde, *Opt. Express*, **2010**, 18, 7670-7677.
2. D. Boateng, C. Hu, Y. Dai, K. Chu, J. Du and Z. J. Smith, *Analyst*, **2022**, 147, 4607-4615.
3. J. T. Hodges, G. Gre´han, G. Gouesbet, C. Presser, *Applied Optics.* **1995**, 34, 2120-2132.
4. C. Marzler, Institut fur Angewandte Physik. **2002**, 02.